Vorogushyn, S., Lindenschmidt, K.-E., Kreibich, H., Apel, H., Merz, B. (2012): Analysis of a detention basin impact on dike failure probabilities and flood risk for a channel-dike-floodplain system along the river Elbe, Germany. - Journal of Hydrology, 436-437, 120-131

DOI: 10.1016/j.jhydrol.2012.03.006

Analysis of a detention basin impact on dike failure probabilities and flood risk for a channel-dike-floodplain system along the river Elbe, Germany

Sergiy Vorogushyn[a], Karl-Erich Lindenschmidt[b], Heidi Kreibich[a], Heiko Apel[a], Bruno Merz[a]

[a]*Deutsches GeoForschungsZentrum GFZ, Section 5.4: Hydrology, Telegrafenberg, 14473 Potsdam, Germany*
[b]*University of Saskatchewan, Global Institute for Water Security, 11 Innovation Boulevard, Saskatoon, SK, S7N 3H5, Canada*

Abstract

Highly concentrated asset values are often protected by dikes stretching along the river course. During extreme floods, dikes may fail due to various breach mechanisms and cause considerable damage. Therefore detention basins are often additionally installed to reduce the flood risk for downstream communities. In such situations, however, the systemic performance of dikes and spatial redistribution of inundation patterns are often unknown. Intuitively expected effects such as more probable breaches downstream due to fewer breaches upstream and consequently higher conveyance of upstream reaches lack evidential proof. With a coupled probabilistic-deterministic 1D-channel - dike breach - 2D-inundation - flood damage model chain the impact of a detention basin on losses to residential buildings and agricultural crops is investigated. We demonstrate the changes in dike performance due to systemic load and relief along the river course on the Middle Elbe, Germany considering three breach mechanisms: overtopping, piping and slope

micro-instability. The reduction of overtopping failures due to the detention basin resulted in the slightly increased breach probabilities due to piping and micro-instability farther downstream. Finally, the uncertainty in hazard and damage estimations are analysed using the Monte Carlo simulation and applying several damage models. Despite high uncertainties in flood hazard and damage estimations, we conclude that the risk reduction to residential buildings downstream of the detention basin exceeds the higher losses to agricultural crops within the filled detention area.
Keywords: flood hydraulics, dike/levee failure, damage modelling, flood risk, flood detention basin

1. Introduction

Detention basins represent retention areas, which are surrounded by dikes and become filled during flood events in order to reduce peak discharges and water levels, aiming at hazard and risk reduction for downstream areas. Detention basin filling can be uncontrolled or activated by human intervention and has to follow a certain strategy in order to achieve an optimum flood peak capping effect. Detention basins are widely used for flood protection purposes in many countries. Particularly, in China they are implemented to cope with floods on large rivers (Shu and Finlayson, 1993; Lin et al., 2010). Unfortunately, we face examples, e.g. along the Yangtze River, where the originally planned flood detention basins experience intensive populating and settlement of industries following the demographic and economic pressures (King et al., 2004).

On the Elbe River in Germany, several detention basins were built during the past century. The detention areas on the Lower Havel River, which is the tributary of the Elbe, were activated during the Elbe flood in August 2002 (LUA, 2002), actually for the first time since their construction in 1930s. Förster et al. (2005) calculated a peak water level reduction by about 40 cm in the Elbe River. Facing the experience during this flood event, an optimisation analysis of the Lower Havel detention areas was undertaken in several research projects taking into account hydrological, hydrodynamic and ecological aspects (Bronstert, 2004; WASY, 2005). The August 2002 flood on the Elbe River also manifested that besides an optimisation of control strategies for existing detention basins, additional retention capacities are required in order to alleviate adverse effects of extreme inundations. Potential retention areas on the Middle Elbe, considered prior to the 2002 flood (Helms et al., 2002), again gained actuality afterwards (IKSE, 2003; IWK, 2004).

Some of these proposed detention basins were analysed by Huang et al. (2007) and Förster et al. (2008a) with the aim to develop a control strategy for an efficient flood peak reduction. Huang et al. (2007) used a quasi-2D modelling approach, where the detention basins are represented as a set of storages interconnected by 1D-channels. Förster et al. (2008a) applied a fully dynamic 1D-2D coupled model for evaluation of detention basin operation. Additionally, Gierk et al. (2008) assessed the flood peak reduction along the Elbe considering 4 detention areas and 22 dike shift measures defined in IKSE (2003) using a diffusion wave channel model and simple storage functions for detention basins. For effective reduction of peak flood stages, the time of gate opening in relation to the phase of a flood wave is crucial (Jaffe and Sanders, 2001; Sanders et al., 2006; Hesselink et al., 2003). The optimal activation time was found to be slightly prior to the peak time by several studies (Jaffe and Sanders, 2001; Sanders et al., 2006; Huang et al., 2007). In the optimal case, the flood hydrograph should be capped utilizing the full storage capacity of a detention basin.

The reviewed studies mainly focused on the assessment of peak water level reduction in a river channel due to flood detention basins using deterministic modelling. The assessment of flood consequences in terms of risk or risk reduction are rare. Particularly, consideration of uncertainties associated with the design floods and dike breaches lack an appropriate treatment, although partly considered in a few previous works. Paik (2008) used the probabilistic methods to determine the probability of exceedance of design peak outflow of a storm water detention basin taking into account the uncertainty in seven design parameters. Chen et al. (2007) additionally estimated the monetary losses due to floods and calculated economic benefits of detention ponds in Taiwan. The authors, however, assessed the effect of uncontrolled ponds filled by rainstorm overland flow rather than by overbank channel flow.

Förster et al. (2008b) estimated the expected annual damage to the agricultural sector and road infrastructure inside a planned detention area on the Middle Elbe for compensation planning. Recently, de Kok and Grossmann (2010) analyzed deterministically the risk reduction in terms of avoided expected annual damage along the main trajectory of the German Elbe part due to various flood control strategies including detention areas. The authors took dike overtopping and breaches due to overtopping into account. In non-diked areas, however, a simple planar surface interpolation was applied to estimate inundation areas. This methodology disregards flood volume that can lead to an overestimation of inundation areas.

In the presented paper, we estimate the benefit of a proposed detention basin on the Middle Elbe in terms of flood damage reduction to residential buildings and agricultural crops along a 91 km Elbe reach. We do not limit us to the evaluation of peak flow/stage reduction but rather consider the flood consequences in terms of flood risk. We apply a 1D-2D coupled hydraulic modelling approach in order to account for the mass transfer between the channel and floodplain in both flow directions. The vast majority of previous studies use the deterministic approach to hazard/risk evaluation. However, in view of considerable uncertainties in flood processes and flood risk models, this approach may introduce a bias into the decision making process. In contrast to the other works, we quantify the uncertainty in risk by considering the uncertainty in inundation depth and duration due to different flood hydrograph shapes, dike breach locations, breach times and widths as well as by taking into account several damage estimation models.

Applying a complex deterministic-probabilistic modelling system, we additionally compute the changes in dike breach probabilities resulting from the load relief of flood protection structures and investigate the systemic effects of the dike performance in the channel-dike-detention basin system. Besides overtopping, we consider piping and slope micro-instability as additional dike failure mechanisms contrary to the previous studies.

2. Methodology

2.1. Study site

For investigation of the impact of a detention basin on dike failure probabilities and flood damage, we selected a 91 km river reach on the Middle Elbe, Germany, between the gauges Torgau and Vockerode (Fig. 1). The reach is nearly fully protected by dikes or is characterized by elevated banks. Two detention basins at Mauken proposed by IKSE (2003) and IWK (2004) were considered in this study. For the sake of simplicity they were aggregated into one entity disregarding an additional control gate between two adjacent parts. We assumed only one inlet opening at the Elbe-km 180. The total maximum capacity was estimated at about $105 \cdot 10^6$ m^3 with a total area of about 28.5 km^2.

The detention basin is activated upon the achievement of the triggering discharge value in the river channel. This discharge was determined for five typical stream hydrograph shapes applying the detention basin control strategy developed by Huang et al. (2007) for this site. We used a fixed opening width of 50 m as suggested by the local authorities and also applied by Förster et al. (2008a). Sanders et al. (2006) investigated the effectiveness of a detention basin operation as a function of hydrographs of different durations/volumes, basin area, gate opening time and opening width.

The opening width was found to have an impact on the capping effect, but it depends on the other three parameters. We therefore relied in the sensitivity analysis done by Huang et al. (2007), who found almost no difference in the capping effect when using the inlet width of 50 and 100 m for this detention basin and the extreme flood event in 2002. With regards to the

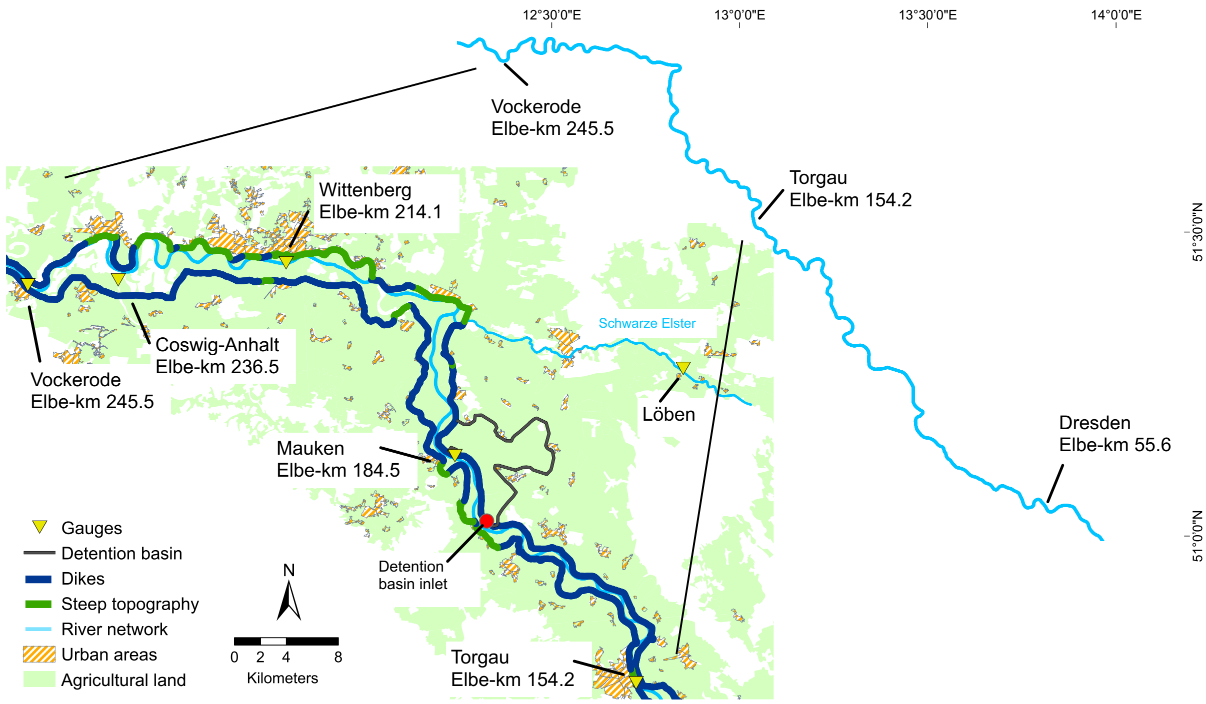

Figure 1: Study area and location of the detention basin.

inlet opening duration, Chatterjee et al. (2008) found very little sensitivity of the river discharge and the water level in a river channel to the durations between 5 and 60 minutes. We used the value of one hour to prevent hydraulic model instabilities due to hydraulic shock.

2.2. Flood hazard and damage models

2.2.1. Inundation Hazard Assessment Model (IHAM)

For the simulation of the flood hazard along a diked river reach, we applied the Inundation Hazard Assessment Model (IHAM) (Vorogushyn et al., 2010) — a hybrid deterministic-probabilistic model for the simulation of channel flow, dike failures and subsequent inundation. IHAM combines a 1D full-

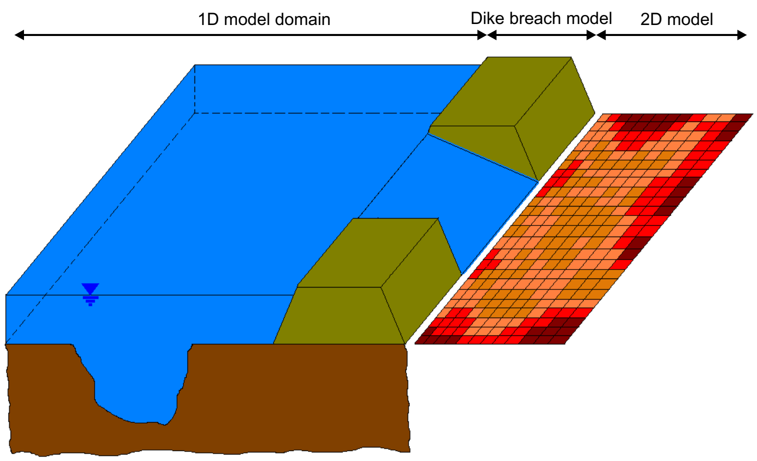

Figure 2: Schematic representation of model domains for each compartment model in the IHAM system.

dynamic wave model (USACE, 1995) for river channel and floodplain between dikes, a probabilistic dike breach model and a 2D diffusive wave storage cell model for hydraulic simulation of overland flow on dike-protected floodplain areas. The schematic representation of modelling domains is shown in Fig. 2.

The 1D model solves the full dynamic St.-Venant equations using the standard four-point numerical scheme and uses the surveyed cross-sections and roughness parametrisation for conveyance description. The two-dimensional flow is computed with the storage cell model that solves the continuity equation (equation 1) and a simplified momentum equation (equation 2) for decoupled fluxes in x and y directions based on the diffusive-wave approximation, as follows

$$\frac{\partial h^{i,j}}{\partial t} = \frac{Q_x^{i-1,j} - Q_x^{i,j} + Q_y^{i,j-1} - Q_y^{i,j}}{\Delta x \Delta y} \tag{1}$$

where $h^{i,j}$(m) denotes the water surface elevation at cell (i, j), t(s) is the time. Here, $Q_x^{i,j}$ and $Q_y^{i,j}$ (m^3 s^{-1}) are fluxes in x and y directions, respectively, and Δx, Δy (m) are cell dimensions ($\Delta x = \Delta y$ for equidistant grid).

$$Q_x^{i,j} = \frac{h_{flow}^{5/3}}{n} \left(\frac{h^{i-1,j} - h^{i,j}}{\Delta x} \right)^{1/2} \Delta y \tag{2}$$

where h_{flow}(m) is the flow depth between two adjacent raster cells, i.e. the difference between the maximum water surface elevation and maximum ground elevation of those cells, n(m$^{-1/3}$ s) is the Manning's roughness coefficient. The equation for the flux in y direction is analogous to Eq. 2, where x and y indices are interchanged and the gradient is computed in y direction.

Although the storage cell model is not capable to adequately capture the flow dynamics behind the dike breaches because of disregarding the local and convective acceleration terms, it is expected to provide a reasonable description of the filling and drainage of the floodplain over the time scale of the flood, as shown in previous studies of floodplain inundation (Horritt and Bates, 2001, 2002). Over the shorter time scale associated with the breaching process and initial movement of the dam-break flood away from the breach, model predictions must be viewed cautiously but this limitation is expected to have little bearing on the final flood area shape and depth distribution which is the focus here. We apply the flow limiter to counteract the oscillations in the numerical solution, which however known for causing some insensitivity to roughness parametrisation (Hunter et al., 2005).

Dike breaches are simulated probabilistically based on the previously developed fragility functions (Vorogushyn et al., 2009, 2010). These functions indicate the failure probability of a dike section depending on hydraulic load (water level and impoundment duration). Fragility functions for overtopping, piping and slope instability due to seepage flow through the dike core (micro-instability) were developed based on the modelling techniques presented in details by Apel et al. (2006) and Vorogushyn et al. (2009) for dikes along the whole river reach. We used historical geometrical and geotechnical dike data partly reflecting the dike status prior to the August 2002 flood event. Contrary to the model setup used in Vorogushyn et al. (2010), new fragility models were used with the recently obtained data on hydraulic conductivity of dike material (LTV, 2010). Currently, significant portions of the dike system are being reinforced or rebuilt by the state authorities.

All three models (1D - dike breach - 2D) are interactively coupled and embedded into a Monte Carlo simulation framework that treats the flood hydrograph shape and dike breach occurrence as random processes. 1D model computes the water stages and discharges at every node with 5 second temporal resolution. Each dike is tested for stability every hour based on the currently computed load. In case, a breach is simulated, the outflow fluxes through the breaches are computed using the drawn weir formula based on the current simulated breach width and water levels in the river channel and adjacent floodplain.

Breach width is stochastically simulated based on predefined probability distribution (Vorogushyn et al., 2010). An outflow volume in the floodplain direction in every time step (5 seconds) is evenly distributed across the so-called interface cells in the 2D model domain adjacent to the breach location. The number of the interface cells (N_{ic}) is defined as a function of the cell size and the current simulated breach width:

$$N_{ic} = \begin{cases} 1 & \text{if } B_w(t) < \Delta x; \\ int(B_w(t)/\Delta x) & \text{if } B_w(t) \geq \Delta x \quad \text{and} \\ & mod(B_w(t), \Delta x) \\ & < \Delta x/2; \\ int(B_w(t)/\Delta x) + 1 & \text{if } B_w(t) \geq \Delta x \quad \text{and} \\ & mod(B_w(t), \Delta x) \geq \Delta x/2. \end{cases} \tag{3}$$

where $B_w(t)$(m) is the breach width at time t.

In case of the backwater flow from the floodplain into the river channel, the discharge is assigned as a lateral boundary condition to the 1D channel node nearest to the dike breach location. We account for continuous interaction between the river channel and floodplain hydraulics, e.g. in case of a filled floodplain, the backwater flow into the channel is considered. We use a mass-conservative solution. However, no momentum transfer from the river channel into the floodplain is considered. It may have a small local impact near the dike breaches, particularly, at dikes not parallel to the channel flow, however, dissipating further outwards. We assume the role of momentum transfer to be negligible with respect to the final shape of the inundation areas, especially for very wide and flat floodplains, where the gravity and pressure forces seem to dominate the water flow compared to the momentum supplied by the channel flow.

IHAM was setup for the study reach between gauges Torgau and Vockerode. The 1D model geometry was described by the surveyed cross-sections spaced at 400 m to 600 m intervals and spanning from one dike to another or to the elevated banks. The rating curve at gauge Vockerode derived by Nestmann and Büchele (2002) was used as the downstream boundary condition. The model was run using the steady-state initial conditions with discharge corresponding to the initial discharge of flood hydrographs.

The roughness coefficients at every cross-section were determined using manual calibration by fitting the steady-state water levels to the observed high water marks from four past flood events. Finally, the model was validated in the steady-state and unsteady mode on the flood event in January 2003. The events ranged between the 2-years to 7-years floods at gauge Torgau (Generalized Extreme Value (GEV) distribution, L-moment method). No further high water marks were available for less frequent events. The Manning's n values were adjusted to minimize the bias and root mean square error (RMSE). In addition, the mean absolute error (MAE) and maximum difference (MD) in water level were computed. The calibrated roughness values ranged between 0.017 $m^{-1/3}$ s and 0.2 $m^{-1/3}$ s, with higher values for the widely extended, vegetated floodplain in the areas of strong river meandering. An overall bias of a few centimeters was obtained (Table 1). The RMSE did not change significantly for the validation run and is in the range of values for the calibration events. In the unsteady run, the peak water stages were underestimated in the range from 0.03 m to 0.53 m.

The detention basin is aimed at peak reduction of severe floods with return period (T) greater than hundred years. We implicitly assumed no damage for flood events with $T < 100$ years implying that the river dikes would withstand the high-probability floods. Floods with $T > 1000$ have extremely low probabilities and are found to contribute little to the annualasied damages for typical floodplains, asset value distribution and vulnerability in

Table 1: Calibration and validation statistics for steady-state 1D hydrodynamic model runs for the reach between gauges Dresden and Vockerode. The statistics are computed for observed and simulated water stages in meters. The flood events in 1995, 1998, 1999 and 2002 were used for calibration. The results of model validation in steady-state are shown for the flood event in 2003. MAE - mean absolute error, RMSE - root mean square error, MD - maximum difference.

Performance statistics	Flood events				
	Jan. 1995	Nov. 1998	Mar. 1999	Feb. 2002	Jan. 2003
Bias	-0.048	-0.004	-0.003	0.032	0.003
MAE	0.16	0.121	0.118	0.101	0.136
RMSE	0.218	0.156	0.161	0.134	0.169
MD	-0.719	0.467	0.566	0.5	0.531

Germany (Merz et al., 2009). Therefore, four return periods of T = 100, 200, 500, 1000 years were investigated in this study.

Flow hydrographs corresponding to these return periods were developed for the gauge Torgau based on the discharge records for the period from 1936 to 2003 adopting the methodology of Apel et al. (2004, 2006). The observed hydrographs of 30 days duration corresponding to the annual maximum discharges - 10 days prior to the peak discharge and 20 days after - were normalized and clustered according to their shape (Vorogushyn et al., 2010). The mean normalized hydrographs (Fig. 3) from five selected clusters were scaled to discharges corresponding to the defined return periods. The latter were determined based on the GEV distribution fitted to the annual maximum discharge series using the L-moment method. The hydrographs for the tributary Schwarze Elster, which correspond to the flood waves in

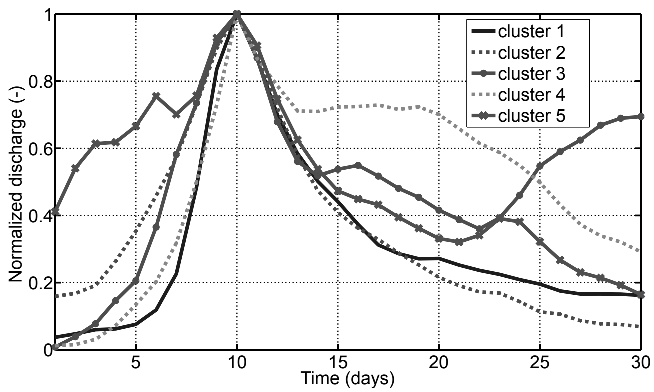

Figure 3: Normalized mean hydrographs corresponding to the five selected hydrograph clusters. The probability of occurrence of each characteristic form is for the cluster 1 - 0.3677, cluster 2 - 0.2352, cluster 3 - 0.1177, cluster 4 - 0.1471, cluster 5 - 0.1323.

the main channel, were also normalized and upscaled to the peak discharges resulting from the regression analysis of the main channel maximum annual discharges and tributary peak flows for corresponding events.

In the Monte Carlo simulation, the input hydrographs were sampled according to their frequency resulting from the cluster analysis (Fig. 3) which characterizes the occurrence of each typical hydrograph shape. Additionally, dike breach locations and times as well as breach widths were treated as stochastic components. The location of dike breaches and point in time, when breach occurs, is determined during the simulation based on actual hydraulic load and fragility curves for each dike section. For each value of the hydraulic load, the fragility curves indicate the probability of dike section failure. Based on this probability, the failure is randomly simulated (failed/not failed) at every time step. The final breach width was sampled from the log-normal distribution function fitted to the sample of 104 observed breaches in

Table 2: Triggering channel flow (Q_{trig}) (m^3s^{-1}) for each hydrograph cluster and respective return period at which the detention basin inlet should be opened.

Return period	100y	200y	500y	1000y
Cluster 1	2412	2900	3476	3995
Cluster 2	2914	3316	3954	4449
Cluster 3	2877	3308	3922	4421
Cluster 4	2669	2966	3508	3932
Cluster 5	3051	3439	4065	4573

the Elbe catchment (Vorogushyn et al., 2010). The observed breach widths ranged between 5 and 340 m, with mean of about 63 m. The full breach width was allowed to develop gradually within one hour.

The detention basin was activated as soon as a certain discharge value at the location of the opening gate was attained. These triggering discharge values were computed depending on the flood wave shape and peak for each hydrograph cluster based on the approach of Huang et al. (2007) and summarized in Table 2. In the operational mode, the operator would receive a lead forecast of peak flow and hydrograph shape. By identifying the corresponding hydrograph cluster, one would obtain the triggering discharge for activation of the detention basin.

The smallest triggering discharges resulted for the hydrograph clusters 1 and 4. They exhibit the narrowest peaks (Fig. 3). Therefore, in order to achieve the maximum discharge capping, the inflow has to be initiated at lower discharges, compared to hydrographs with gentler rising and falling limbs.

For this modelling study, no controlled detention basin emptying was considered. However, backwater flow into the river can occur through the opening and dike breaches, which were allowed anytime on the interface between the Elbe channel and detention basin. The overtopping flow over the river dikes without dike failures was not taken into account.

Two-dimensional flow inside the detention area as well as inundation front propagation caused by dike failures were simulated with the 2D storage cell code. A 50 m $\times$ 50 m digital elevation model was used in this study. The only available inundation area extent from the August 2002 flood event appeared to be insufficient to constrain the roughness parameter during calibration. This inundation resulted from a very complex pattern of the flows through dike breaches and tributary backwater. This could hardly be replicated in the model due to lack of exact data on breach times and development. The distributed roughness parameters were therefore defined for different ATKIS (Official Topographic-Cartographic Information System) land use classes using literature values (Chow, 1959). The proposed detention basin was integrated into the DEM and surrounded by dikes.

A set of 500 IHAM simulation runs was carried out for each return period with and without the projected detention basin. These scenarios are further referred to as 100y, 200y, 500y and 1000y without detention basin, as well as 100ydb, 200ydb, 500ydb and 1000ydb deploying the detention area.

2.2.2. Damage modelling and risk calculation

Inundation patterns indicating water depth distribution and inundation duration were supplied as input data to the damage assessment models for the private and agricultural sectors. Direct economic damages to residential buildings were estimated by four different models to take uncertainty of damage estimation into account: the multifactorial Flood Loss Estimation MOdel for the private sector — FLEMOps and three different depth-damage curves. FLEMOps was developed on basis of empirical damage data from the 2002 flood in the Elbe and Danube catchments and was successfully validated at the Elbe river (Büchele et al., 2006; Thieken et al., 2008; Apel et al., 2009). It is a rule based model, which calculates the damage ratio of residential buildings for five classes of inundation depths (<21 cm, 21-60 cm, 61-100 cm, 101-150 cm, >150 cm), three distinct building types (one-family homes, (semi-)detached houses, multifamily houses) and two categories of building quality (low/medium quality, high quality). Thieken et al. (2005) presented a detailed analysis of the influence of these factors on flood damages. For the application of FLEMOps on the meso-scale, i.e. on basis of CORINE land cover units (DLR and UBA, 2000), a scaling procedure was developed (Thieken et al., 2006). By means of geo-marketing data from INFAS Geodaten (2001) and cluster analysis, the mean building composition and mean building quality per municipality were derived and are available as GIS raster data with a resolution of 25 m for whole Germany.

The depth-damage curves used have been developed for flood action plans or in risk mapping projects for the Rhine catchment (MURL, 2000; ICPR, 2001; HYDROTEC, 2001, 2002). They are commonly used in Germany, however, it remains unclear how they were developed and why they are different although they rely on the same background data, namely the German flood damage database HOWAS (Merz et al., 2004). MURL (2000) calculates the damage ratio of residential buildings by the equation $y = 0.02x$ where x is inundation depth [m] and y is damage ratio [-]. For inundation depths of more than 5 m the damage ratio is set to 0.1 (i.e. 10%). ICPR (2001) estimates the damage ratios of residential buildings by the relation $y = (2x^2 + 2x)/100$. HYDROTEC (2001, 2002) use the root function $y = (27\sqrt{x})/100$. In the latter two models, damage ratios > 1 are set to 1.

All models were applied on the basis of CORINE land cover units (DLR and UBA, 2000) with resolution of 25 m. First, the damage models were applied to the inundation scenarios in order to estimate the damage ratio per grid cell. These ratios were then each multiplied by the specific asset value assigned to the corresponding grid cell. The total asset value of residential buildings was taken from the work of Kleist et al. (2006), who calculated the replacement values for the reference year 2000. Since only the total asset sum was provided for each municipality, the assets are disaggregated on the basis of the CORINE land cover data (DLR and UBA, 2000) following the approach of Mennis (2003).

Using the residential building price index published by the Federal Statistical Agency, the asset values were referenced to the year 2005, which was taken as a basis year for damage calculation. Besides the total damage values for each particular scenario, an expected annual damage (EAD) was computed by integrating the area under the risk curve between scenarios corresponding to the 100-year and 1000-year events (Eq. 4).

$$EAD = \sum_{j=1}^{k} \Delta P_j D_j \tag{4}$$

where ΔP_j and D_j are the exceedance probability increment and the average flood damage for the j-th interval, respectively, and k is the number of increments (here k=4, since scenarios corresponding to the return periods of T = 100, 200, 500, 1000 were used).

The model used to calculate the expected damages to agricultural crops was developed by Kuhlmann (2010). It is based on a monthly disaggregation of the agricultural damages. The model was already applied by Förster et al. (2008b) to compute the losses inside the planned detention area. On the contrary, we apply the model to the whole model domain, also to assess the damages outside the detention basin. The model considers damages to crops, and the expected damage [€ yr^{-1}] for one scenario is calculated by multiplying the probability of occurrence by the damage costs:

$$ED = MV \cdot A \sum_{m=1}^{12} PM_m DI_m \tag{5}$$

where ED is expected damage [€ yr^{-1}] for a particular return period or scenario, MV is market value [€ ha^{-1}], PM_m is probability of flooding for a certain month each year m [yr^{-1}] and DI_m is damage impact on crops for month m [%], and A is affected area [ha].

DI_m depends on the crop type, month of flood occurrence and inundation duration. The differentiation in crop types is necessary since some crops are more prone to flood damages than others. For example, root crops are more susceptible to floodwaters than grain crops. The degree of impact also depends on the vegetative stage of the plant during the time of flooding. The highest damages are expected to occur on mature crops close to the beginning of harvesting since losses cannot be compensated by plant recovery or a second seeding. Water saturation of soil for extended periods of time inhibits plant growth and compromises the integrity of the plant structure.

Table 3: Area, distribution and market value of the main crops for the administrative region of Wittenberg averaged over the years 2000 to 2005.

Crop	Area [ha]	Area fraction [%]	Market value [€ ha^{-1}]
wheat	11128	15.3	704
rye	9994	13.8	459
barley	5698	7.8	605
corn	8307	11.4	883
canola	10128	14.0	632
potatoes	1088	1.5	2339
sugar beets	988	1.4	2103
grass	13999	19.3	266
vegetables I	298	0.4	11227
vegetables II	298	0.4	15799

The impact of floods to root crops and grain crops are categorized in four groups of inundation duration: 1 - 3 days, 4 - 7 days, 8 - 11 days and $>$ 11 days. The damage impact factors were taken from LfUG (2005) and are exemplarily listed by Förster et al. (2008b).

The market value MV in Eq. 5 differs from region to region since the crop yield depends on the climatic and soil conditions and the type of agricultural management practices used. Germany can be subdivided into 38 administrative regions, each of which has different MV for each crop. The market values for the administrative region of Wittenberg, in which our detention basin study site lies, are given in Table 3 for selected crops.

Since the exact spatial allocation of crops was not known and may change from year to year, the crops were distributed randomly in a Monte Carlo simulation (1000 runs) over the agricultural land surfaces maintaining the percentage amounts for each crop given in Table 3. Thus, for every raster cell, the median crop value was obtained and used for damage assessment.

Since the vulnerability is accounted on a monthly basis, the probability of flooding PM needs to be determined for each month m to calculate the expected annual damage for each of the simulated return periods (T = 100, 200, 500 and 1000 years). The time series of the annual maximum discharge from the gauge at Torgau for the time period from 1936 to 2004 was used for the monthly flood frequency analysis. The GEV distribution using L-moments was fitted to the data.

Finally, to make the EADs for residential buildings and agricultural crops comparable, the EAD value integrating all considered return periods is calculated by adopting Eq. 6 to the agricultural damages considering monthly probabilities:

$$EAD = MV \sum_{m=1}^{12} \sum_{j=1}^{k} \Delta P_{mj} DI_m A_j \tag{6}$$

where ΔP_{mj} is exceedance probability increment for the j-th interval and month m, and A_j is average affected area for the $j-th$ interval.

3. Results and discussion

3.1. Impact on river discharge hydrographs

Discharge hydrographs at four selected locations at various distances downstream of the basin inlet were simulated for investigated scenarios. The difference in the median discharge between scenario sets with and without detention basin is expressed in terms of percental change with respect to the scenario without basin (Fig. 4). For all scenario sets at Elbe-Km 184.5, the difference in the median discharge is zero in the first approx. 180 hours. After approx. 180 hours, the reduction of the median discharge by a few percent is attributed to the retention effect of the detention basin. The discharge decline at Elbe-Km 184.5 appears to be similar for all four scenarios, while at the downstream control points the discharge behaviour is different exhibiting not only decrease but also increase. This depends on the performance of dikes.

The increase of discharge after activation of the detention basin in some scenarios and locations (e.g. scenario $500y$ at Elbe-km 214.1) could be interpreted as an indication for enhancement of dike stability. At Elbe-km 214.1 for scenarios $100y$ and $200y$ nearly no change in median flow is simulated after 300h. This is a consequence of almost no influence of the detention basin on dike stability between Elbe-km 184.5 and 214.1. This is confirmed by little changes in breach probabilities at this river stretch shown in Figs. 5a, b. For the $500y$ and $1000y$ scenarios, the effect of the detention basin on breach probabilities is already visible upstream of Wittenberg (Elbe-km 214.1) (Figs. 5c, d) with some positive and some negative differences. This results in changes of median discharge at Elbe-km 214.1. Due to capping of the peak discharge, dike breach probabilities are mainly reduced downstream of the detention basin for all flood magnitudes (Fig. 5). Therefore, higher average discharges are modelled in the river channel at downstream locations after basin filling, since more water passes through the channel that otherwise would spill into the hinterland.

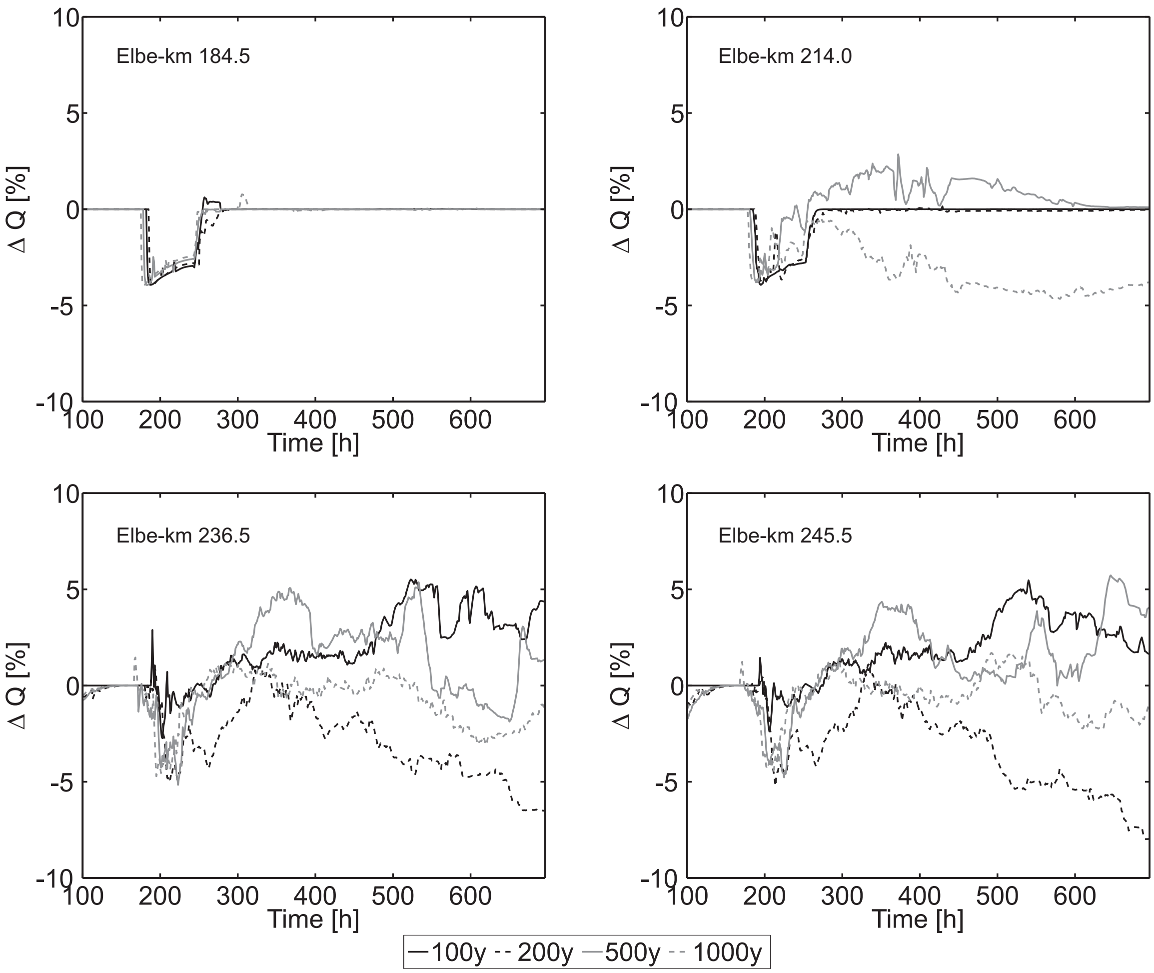

Figure 4: Difference in median discharge between the four flood scenarios with and without the detention basin at four different locations along the study reach. The difference is given in [%] compared to the discharge of scenarios without the basin.

The fluctuating behaviour of hydrographs suggests a complex interplay between dike failures at different parts of the reach and river sides. It is the interaction of loading and relief that explains this pattern. However, at this stage we cannot interpret all fluctuations of discharge along the river channel. It is conjectured that such a behaviour results from different temporal redistribution of dike failures in the simulation time window. However, the breach frequency maps (Fig. 5) are not able to manifest this suggestion, since they represent an overall static picture of the system state. Representation of breach frequencies as a function of time, i.e. how often breaches at certain location occur at various time windows during the course of simulation, would provide an insight into the system dynamics and is the subject for future research. Moreover, the storage volume in the floodplain compartments behind the dikes influences the flow hydrograph, i.e. it is not only necessary to have more frequent breaches at some places but also sufficient storage capacity in order to significantly reduce the river discharge.

3.2. Impact on dike breach probabilities

Monte Carlo simulations with IHAM resulted in the generation of probabilistic dike hazard maps. These maps indicate the probability of failure of each dike section for all scenarios (Fig. 5). The Monte Carlo runs converge to the level of $\pm 3\%$ *points* for additional 10% of runs, i.e. additional 50 runs lead to changes in breach probabilities of $\pm 3\%$ *points*. This explains the variable probability changes for dike breaches upstream of the detention basin, where any influence is expected.

The deployment of the projected detention basin leads primarily to a reduction of dike breach probabilities (up to 36% *points*) for all magnitude sce-

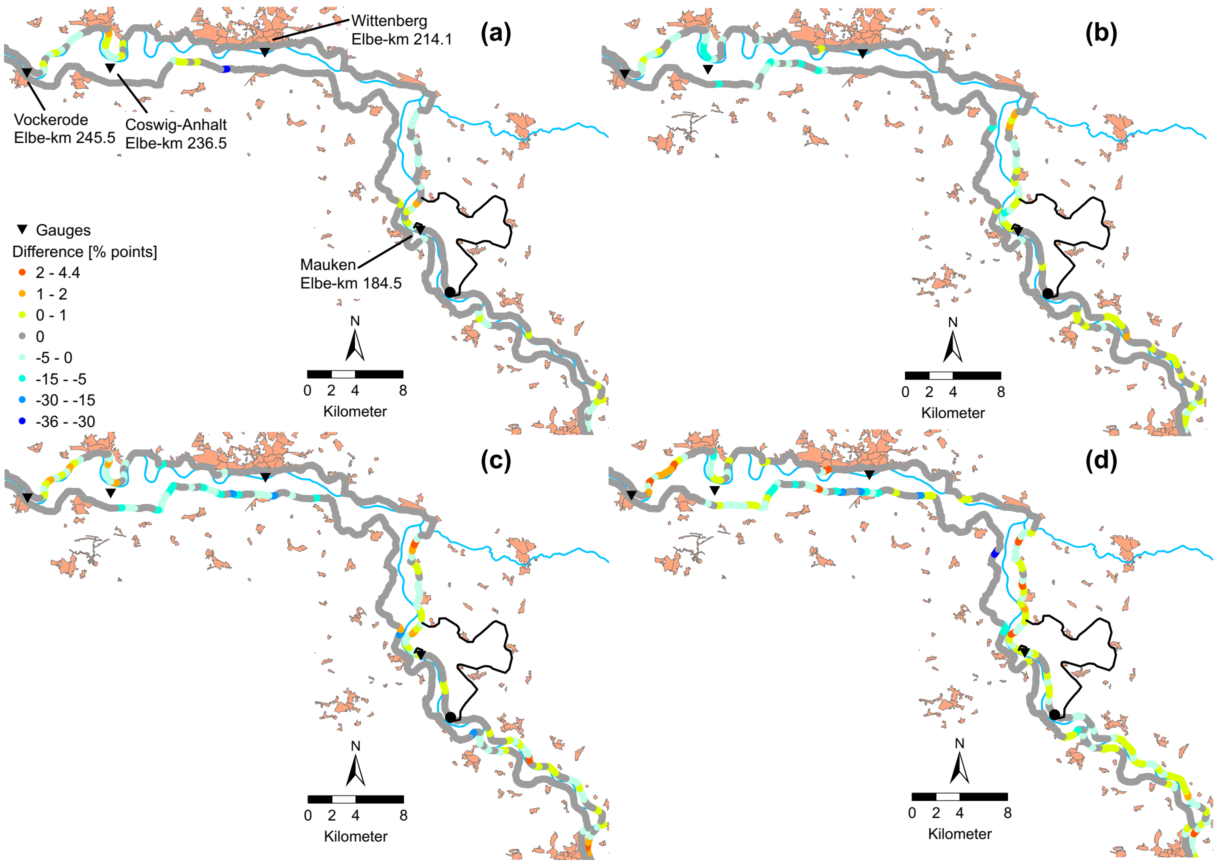

Figure 5: Difference in dike failure probabilities between the flood scenarios (a) 100ydb and 100y, (b) 200ydb and 200y, (c) 500ydb and 500y, and (d) 1000ydb and 1000y. Legend in (a) applies to (b), (c) and (d).

narios (Figs. 5). The reduction is more pronounced in scenarios for T = 200, 500 and 1000 years. The reduction of dike failures is mainly clustered on the left-side dike stretch opposite to the City of Wittenberg. Additionally, less frequent breaches are detected for some dike sections opposite to the detention basin. A few dike sections are exposed to more frequent failures. However, the increase is very weak and nearly at the level of noise of $\pm 3\%$ *points*. The slight increase in dike breach probabilities (up to 4.4% *points*) is spatially clustered at the end of the reach for scenarios with T = 500 and 1000 (more frequent breaches indicated in red and orange in Figs. 5c,d), which is due to the higher flows (Fig. 4) at this location (Elbe-km 245.5). This is a consequence of increased stability of upstream dikes. Closer scrutiny of this pattern is provided by the disaggregation of probabilities according to breach mechanisms exemplified for the 500*db* scenario (Figs. 6a, b, c).

We question, whether the deployment of the detention basin results in shifts in frequency of breach mechanisms, e.g. whether the reduction of overtopping frequencies leads to increase of frequencies of piping and micro-instability. It becomes evident that considerable reduction of dike failure probabilities is primarily due to overtopping (Fig. 6a). It is conjugated with the very weak but spatially agglomerated increase of breach frequencies due to piping and slope micro-instability (Figs. 6b, c). Those agglomerations are detected mainly for the dike sections which are located near or farther downstream of dikes with reduced overtopping frequencies (downstream of Wittenberg). This pattern suggests that the decrease in overtopping failure probability, which reacts sensitively to the detention basin deployment, leads to the lower water level extremes. This slightly enhanced stability of non-

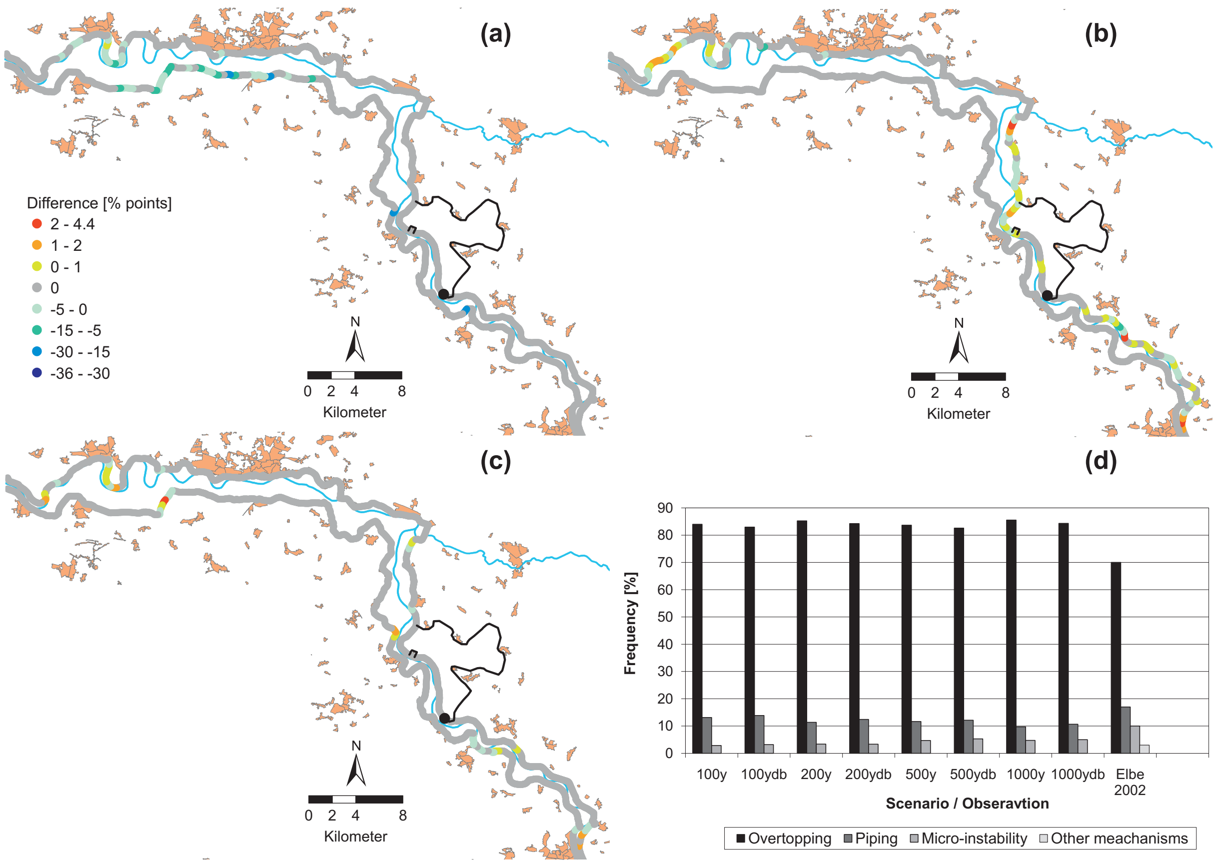

Figure 6: Difference in dike failure probabilities between the flood scenarios $500ydb$ and $500y$ for (a) overtopping, (b) piping and (c) micro-instability breach mechanisms. Legend in (a) applies to (b) and (c). (d) Relative frequency of considered dike breach mechanisms responsible for dike failures in simulated scenarios with and without the detention basin. Relative frequency of observed breaches in the Elbe catchment during the 2002 flood event.

overtopped dikes resulted in the greater average load in terms of water level and duration. This impels a very weak but spatially agglomerated increase of dike failures due to piping and micro-instability downstream of Wittenberg that is manifested in the total increasing breach probabilities (Figs. 5b, c).

This result is further confirmed by the small changes in relative frequency of mechanisms responsible for dike failures (Fig. 6d). The diagram indicates a slight decrease of overtopping failure frequency in favor of piping and micro-instability, when scenarios of corresponding magnitudes with and without the detention basin are compared. Generally, there are only little variations in breach frequencies across the scenario set. There seems to be no significant impact of flood magnitude on the distribution of failure mechanisms. The simulated mechanism frequency is similar to the one observed during the 2002 flood in the Elbe catchment, although overtopping is somewhat overestimated.

The detention basin was shown capable to considerably reduce the breach probability due to overtopping for several dike sections, typically in the range from 5 to 25% *points*, locally up to 36% *points*. Simultaneously, very slight but spatially agglomerated increase in failure probabilities due to piping and slope micro-instability were detected. The net effect of the breach frequency alteration on the flood hazard is explored in the next section.

3.3. Impact on flood hazard

IHAM computes probabilistic flood hazard maps which display, for each scenario, the flood intensity indicators (e.g. maximum inundation depth and duration) for different percentiles. For each raster cell, median and uncertainty range for maximum inundation depths and durations are computed in the Monte Carlo framework. Figures 7a,b provide an example of median maximum inundation depths and durations for the scenario $500y$ as well as corresponding dike failure probabilities. The impact of detention basin deployment on flood hazard was analysed in terms of changes in inundation depth and duration. These flood intensity indicators are decisive for direct economic damages to residential buildings and to agricultural crops.

The deployment of the detention basin results mainly in the reduction of the median maximum inundation depths, as shown for the comparison of the 500-year scenarios (Fig. 7c). Obviously, the area inside the basin experiences much more intensive inundation when flooded intentionally which is emphasized in the increase of the median maximum depths inside the basin (generally up to $0.5 - 2$ m, with higher level of up to > 4 m in local depressions). The comparison of the respective scenarios with and without the detention basin indicates a hazard relief for downstream areas in terms of maximum water depth (up to 2.82 m for the median maximum depth). The vast majority of the inundated areas in the downstream half of the reach experienced a decline of maximum water depths. The strongest hazard relief is attained directly downstream of the detention basin and closely to the dike sections with reduced overtopping probability near Wittenberg (Fig. 6a). The map for median inundation duration exhibits widely similar patterns as the map for median maximum inundation depth (Figs. 7d). Generally, in the areas of decreasing maximum water depth, inundation duration also decreases.

The analysis carried out in this section showed that the deployment of the detention basin has a potential to reduce maximum inundation depth and

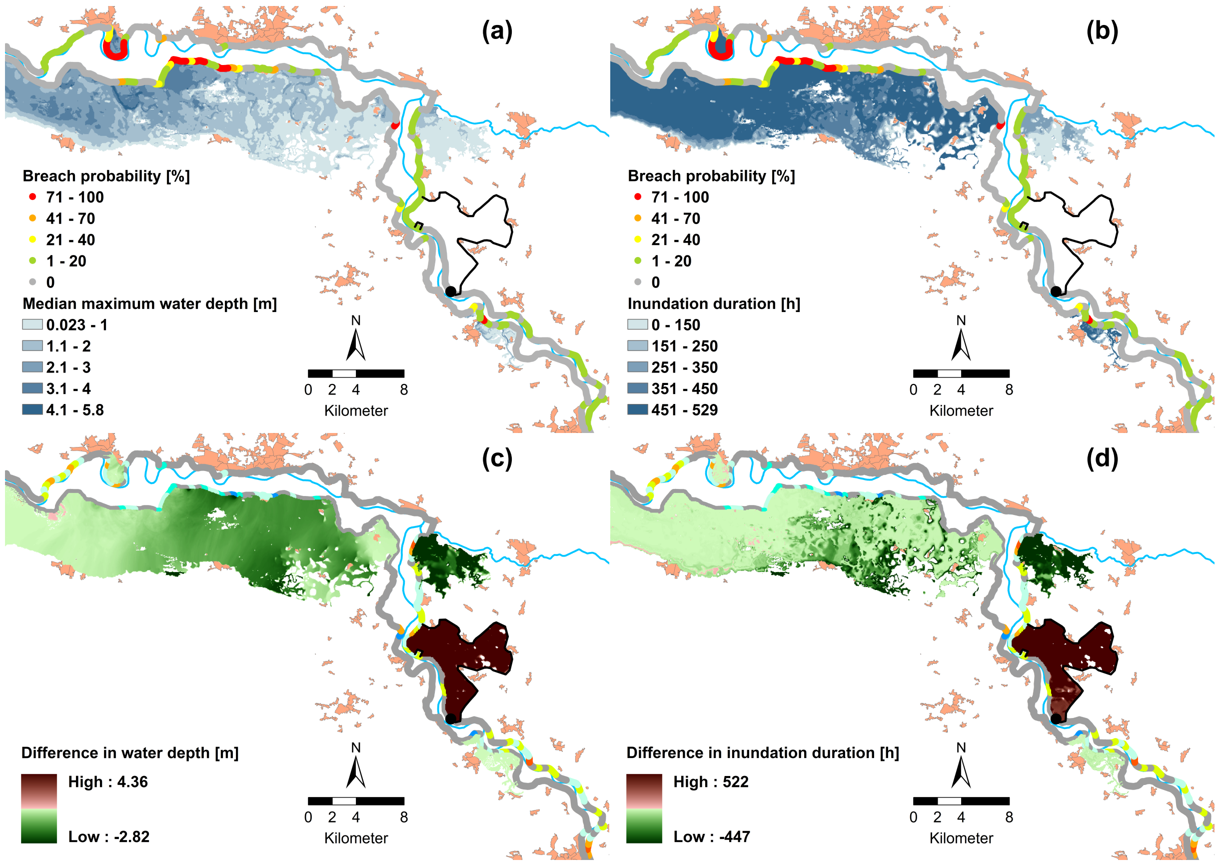

Figure 7: Dike breach probabilities and median maximum inundation (a) depth and (b) duration for the scenario 500y. Difference between the scenarios 500ydb and 500y in (c) median maximum inundation depths and (d) median inundation duration.

duration for downstream parts of the reach. However, a more severe hazard is to be expected inside the detention basin due to controlled flooding. Whether the redistribution of the hazard is economically bearable can be determined by analyzing the expected damages.

3.4. Uncertainty in loss estimation and impact on flood risk

Flood risk is defined by the product of the event probability and its consequence. We assess the consequence of flood in terms of direct economic damages. The damage models for residential buildings and agricultural crops described in Sect. 2.2.2 were used to compute the damage in monetary terms. Fig. 8 presents the summary of inundation losses across all scenarios and damage models for residential buildings.

The uncertainty in losses represented in Fig. 8 is attributed to the uncertainty in hazard and uncertainty in damage modelling. The uncertainty in hazard modelling resulting from uncertainty in flood wave shape (using a single extreme value model) and dike breach stochasticity (dike breach location, breach time and breach width) is represented by the $10^{th} - 90^{th}$ percentile range of each bar. The uncertainty in damage modelling for one scenario is given by the maximum range of losses across all bars, i.e. across all damage models, for a certain percentile. For example, consider for the 100y-scenario the median value at all bars corresponding to different damage models (Fig. 8). The value range MURL-median – HYDROTEC-median represents the uncertainty due to the selection of a damage model.

It becomes apparent that the uncertainty in flood risk is dominated by the uncertainty in damage estimation compared to the uncertainty in hazard. This conclusion was already drawn by Apel et al. (2009), who considered

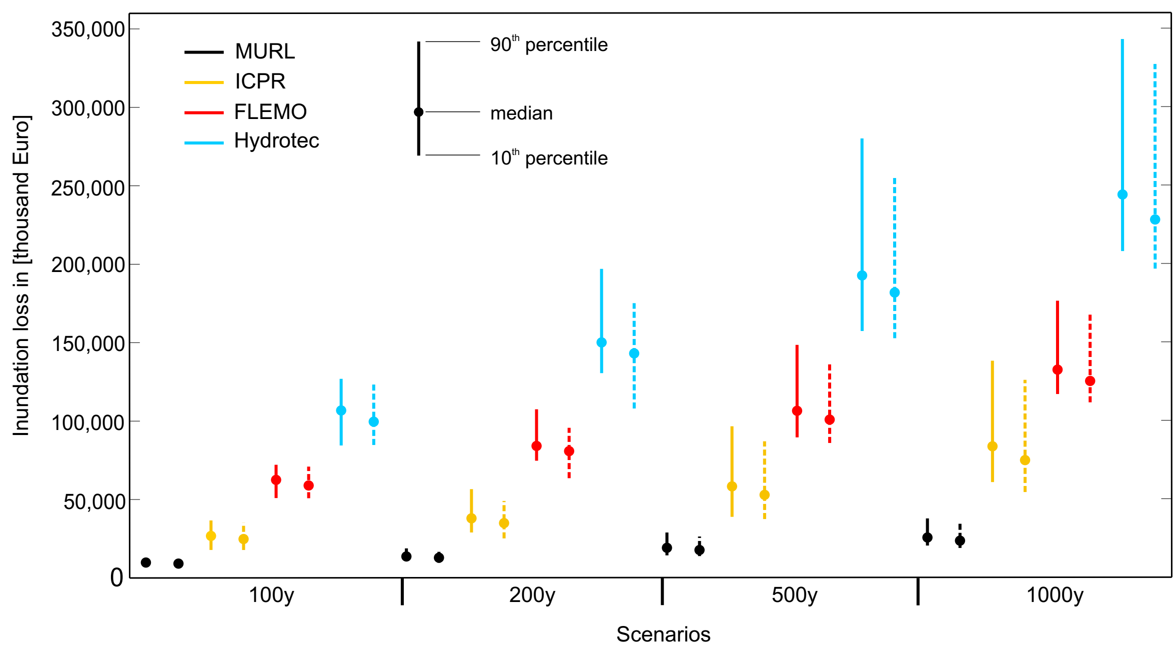

Figure 8: Flood losses to residential buildings computed by different damage models. Solid and dashed lines represent scenarios without and with the detention basin, respectively.

hydraulic and damage models of different complexity to estimate the risk. Merz and Thieken (2009) found, however, in case of the City of Cologne that uncertainty in hazard due to choice of the statistical model for extreme values and inundation models exceeds the uncertainty in damage models.

The uncertainty in losses due to hazard estimation and damage models increases with flood magnitude. This is expressed by longer bars and larger range of respective percentiles for high-magnitude scenarios compared to the lower ones (Fig. 8). The differences in loss estimation by different damage models increase with increasing flood magnitude. This can be explained by the different slopes of the damage curves used in different models (see e.g. Apel et al. (2009)), i.e. with increasing flood depths the proportional increase in damage is different across models. The uncertainty in flood losses due to the uncertainty in hazard grows as well with increasing scenario magnitude (Fig. 8).

This uncertainty is controlled by the flood wave shape and dike breach stochasticity. Upscaling the normalized flood hydrographs (Fig. 3) to different return periods, one changes the flood volume (the area under the flood hydrograph curve) unproportionally for different hydrograph clusters. This unproportional change partly contributes to the larger interpercentile range (10^{th}–90^{th} percentiles) for higher return periods. The other three uncertainty sources — breach location, breach point in time and breach width — are responsible for volume redistribution in space. For lower magnitude events, dike breaching processes exhibit more randomness and have a stronger influence on uncertainty in hazard (Vorogushyn et al., 2010). With increasing flood magnitude, randomness of failures reduces, i.e. in a fixed number of

Monte Carlo runs breach patterns converge faster. Hence, the variability in flood hydrograph volume exhibits an increasing influence on uncertainty in losses with increasing flood magnitude.

The deployment of the detention basin led generally to a reduction of damages to residential buildings for all damage models. The damages corresponding to high percentiles were stronger reduced than those corresponding to the lower percentiles. The result seems to be logical, since the detention basin buffers higher discharges more strongly, discharges that would otherwise cause more frequent breaches and high damages.

Additionally, we computed the avoided expected annual damage in both asset classes, residential buildings and agricultural crops, in order to evaluate the benefit of the detention basin (Table 4). In this way, the impact on the different sectors was made comparable since the damages to the agricultural sector cannot be expressed as single event flood damage in a certain year because of the dependence on the month of occurrence. The results manifest the already observed stronger reduction of the high-percentile damages across all models for the private sector. It becomes evident that the deployment of the detention basin leads to an increased EAD in the agricultural sector in our modelling exercise. The losses to agricultural crops in the vicinity of the detention area cannot be compensated by the reduction of the flooded areas and inundation durations further downstream. However, the savings in EAD for the private sector exceed the losses in the agricultural sector based on three of the four damage models. Only the median of the MURL damage function, known for considerable underestimation of flood damages (Thieken et al., 2008) indicated lower savings than expected loss increases.

Table 4: Reduction in EAD [thousand € yr^{-1}] over all scenarios and percentiles

Damage model/Sector	10^{th} percentile	median	90^{th} percentile
MURL	8.19	8.97	16.08
ICPR	21.51	32.41	59.2
FLEMOps	54.61	37.13	78.19
Hydrotec	104.31	75.78	148.82
Agricultural sector	-7.87	-15.42	-4.77

When comparing the avoided EAD using the FLEMOps model — the only validated damage model for the Elbe catchment — the savings across all percentiles compensate the losses in the agricultural sector. Particularly, the median and the 90^{th} percentile of the avoided EAD manifest considerable positive balance. It means that with the probability of 50 %, one would attain a considerable positive avoided EAD value.

4. Conclusions

The IHAM methodology was applied for the assessment of a detention basin impact on flood wave, dike breach probability and inundation hazard. The effect of the detention basin deployment was tested for extreme flood scenarios with return periods of 100, 200, 500 and 1000 years. Different changes in patterns of dike breach probabilities were modelled and are associated with the systemic effect of dike load and relief due the deployment of the detention basins. With respect to flood damage and risk, residential buildings and agricultural crops were taken into account.

We systematically analyzed the uncertainty in the computation of hazard and damage taking into account the following aspects. The uncertainty in hazard is associated with the uncertainty in flood hydrograph shape for a particular return period, dike breach location, breach time and ultimate breach width. The investigated uncertainty in the damage estimation originates from uncertainty in susceptibility represented by different applied damage functions or models. Uncertainties associated with exposure were not taken into account. Still, differences between the building damage estimates from the different models are large. It was demonstrated that in this case, the uncertainty due to the selection of a damage model exceeds the uncertainty in losses due to uncertain hazard estimation. Nevertheless, we can conclude that even using very simplified assumptions about the design and operation of the proposed detention basin, which do not guarantee the highest benefit, the tangible benefit in terms of the avoided expected annual damage for private households exceeds the higher possible damages to the agricultural sector. The latter result from a controlled flooding of the detention basin and cannot be compensated by the avoided damages to the agricultural crops in the downstream part of the reach.

The general result for the flood risk reduction due to the detention basin would probably hold or even a stronger reduction would be achieved, if further economic sectors (e.g. infrastructure, industry) are taken into account in damage estimation. Since there is only agricultural use inside the detention basin, this is the only sector expecting higher flood damages due to the deployment of the basin. Flood damage of all other sectors will be reduced due to the lower flood intensity, i.e. lower maximum depths and shorter inundation durations, downstream.

In this particular test study, the uncertainty in damage modelling did not substantially affected the final conclusion about the effectiveness of the detention basin. However, we have demonstrated the huge uncertainty range across the damage models which may become prohibitive in other cases. We therefore advocate the use of the multifactorial damage model FLEMOps, which has been shown to outperform simple depth-damage functions particularly in the Elbe catchment, for which it has been successfully validated (Thieken et al., 2008; Kreibich and Thieken, 2008). Additionally, we plea to a more extensive validation of damage models across different river basins. At this point, we stress the necessity to systematically collect the post-flood damage-related data in a consistent form as for instance suggested in the HOWAS21 flood damage database (Thieken et al., 2009) and also advocated by Elmer et al. (2010) in order to be used for damage model development and validation.

Despite the fact that it is always difficult to generalise or transfer the results of a flood risk analysis to another region, one can speculate that generally the controlled use of a detention basin will lead to a flood risk reduction if it is appropriately planned and operated, i.e. asset values downstream of the basin can be saved due to the retention of water and if the land use within the basin is strictly limited to low value agricultural use over a long time.

5. Acknowledgements

The authors are grateful to the LHW Sachsen-Anhalt, LTV Sachsen and Federal Institute of Hydrology (BfG) for provision of dike and detention basin data. Geoinformation (DEM-D-50, DEM-D-25, ATKIS) is provided by Vermessungsverwaltung der Bundesländer und BKG (www.bkg.bund.de).

References

Apel, H., Aronica, G.T., Kreibich, H., Thieken, A.H., 2009. Flood risk analyses — how detailed do we need to be? Natural Hazards 49, 79–98. doi:10.1007/s11069-008-9277-8.

Apel, H., Thieken, A.H., Merz, B., Blöschl, G., 2004. Flood risk assessment and associated uncertainty. Natural Hazards and Earth System Sciences 4, 295–308.

Apel, H., Thieken, A.H., Merz, B., Blöschl, G., 2006. A probabilistic modelling system for assessing flood risks. Natural Hazards 38, 79–100. doi:10.1007/s11069-005-8603-7.

Bronstert, A.E., 2004. Möglichkeiten der Minderung des Hochwasserrisikos durch Nutzung von Flutpoldern an Havel und Oder. Schlussbericht zum BMBF-Projekt im Rahmen des Vorhabens "Bewirtschaftungsmöglichkeiten im Einzugsgebiet der Havel". Institut für Geoökologie, Universität Potsdam. In German.

Büchele, B., Kreibich, H., Kron, A., Thieken, A.H., Ihringer, J., Oberle, P., Merz, B., Nestmann, F., 2006. Flood-risk mapping: contributions towards an enhanced assessment of extreme events and associated risks. Natural Hazards and Earth System Sciences 6, 485–503.

Chatterjee, C., Förster, S., Bronstert, A., 2008. Comparison of hydrodynamic models of different complexities to model floods with emergency storage areas. Hydrological Processes 22, 4695–4709. doi:10.1002/hyp.70792.

Chen, C.N., Tsai, C.H., Tsai, C.T., 2007. Reduction of discharge hydrograph and flood stage resulted from upstream detention ponds. Hydrological Processes 21, 3492–3506. doi:10.1002/hyp.6546.

Chow, V.T., 1959. Open Channel Hydraulics. McGraw-Hill, New York, USA.

DLR and UBA, 2000. CORINE Land Cover 2000. Daten zur Bodenbedeckung Deutschland (Data on land cover Germany). German Aerospace Center, German Remote Sensing Data Center. The Federal Environment Agency. Oberpfaffenhofen, Berlin, Germany.

Elmer, F., Seifert, I., Kreibich, H., Thieken, A.H., 2010. A Delphi method expert survey to derive standards for flood damage data collection. Risk Analysis 30, 107–124. doi:10.1111/j.1539-6924.2009.01325.x.

Förster, S., Chatterjee, C., Bronstert, A., 2008a. Hydrodynamic simulation of the operational management of a proposed flood emergency storage area at the Middle Elbe River. River Research and Applications 24, 900–913. doi:10.1002/rra.1090.

Förster, S., Kneis, D., Gocht, M., Bronstert, A., 2005. Flood risk reduction by the use of retention areas at the Elbe River. International Journal of River Basin Management 3, 21–29.

Förster, S., Kuhlmann, B., Lindenschmidt, K.–E., Bronstert, A., 2008b. Assessing flood risk for a rural detention area. Natural Hazards and Earth System Sciences 8, 311–322.

Gierk, M., Bodis, K., Younis, J., Szabo, J., De Roo, A., 2008. The impact of retention polders, dyke-shifts and reservoirs on discharge in the Elbe river. JRC Scientific and Technical Report JRC 49172. JRC Joint Research Centre. doi: 10.2788/68635.

Helms, M., Büchele, B., Merkel, U., Ihringer, J., 2002. Statistical analysis of the flood situation and assessment of the impact of diking measures along the Elbe (Labe) river. Journal of Hydrology 267, 94–114.

Hesselink, A.W., Stelling, G.S., Kwadijk, J.C.J., Middelkoop, H., 2003. Inundation of a Dutch river polder, sensitivity analysis of a physically based inundation model using historic data. Water Resources Research 39, 1234. doi:10.1029/2002WR001334.

Horritt, M.S., Bates, P.D., 2001. Predicting floodplain inundation: raster-based modelling versus finite element approach. Hydrological Processes 15, 825–842.

Horritt, M.S., Bates, P.D., 2002. Evaluation of 1D and 2D numerical models for predicting river flood inundation. Journal of Hydrology 268, 87–99.

Huang, S., Rauberg, J., Apel, H., Disse, M., Lindenschmidt, K.–E., 2007. The effectiveness of polder systems on peak discharge capping of floods along the middle reaches of the Elbe River in Germany. Hydrology and Earth System Sciences 11, 1391–1401.

Hunter, N.M., Bates, P.D., Horritt, M.S., De Roo, P.J., Werner, M.G.F., 2005. Utility of different data types for calibrating flood inundation models within a GLUE framework. Hydrology and Earth System Sciences 9, 412–430.

HYDROTEC, 2001. Hochwasser-Aktionsplan Angerbach (Flood action plan for the river Angerbach). Teil I: Berichte und Anlagen. Study in order of the National Environmental Agency of the city of Düsseldorf. Aachen, Germany. In German.

HYDROTEC, 2002. Hochwasser-Aktionsplan Lippe (Flood action plan for the river Lippe). Teil I: Berichte und Anlagen. Study in order of the National Environmental Agency of the city of Lippstadt. Aachen, Germany. In German.

ICPR, 2001. Atlas on the risk of flooding and potential damage due to extreme floods of the Rhine. Technical Report. International Commission for the Protection of the Rhein. Koblenz, Germany.

IKSE, 2003. Aktionsplan Hochwasserschutz Elbe. Technical Report. Internationale Kommission zum Schutz der Elbe. 79 pp.

INFAS Geodaten, 2001. Das Data Wherehouse. INFAS GEOdaten GmbH. Bonn.

IWK, 2004. Untersuchung von Hochwasserretentionsmaßnahmen entlang der Elbe im Bereich der Landkreis Wittenberg und Anhalt-Zerbst (Kurzfassung). Technical Report. Institut für Wasserwirtschaft und Kulturtechnik, Universität Karlsruhe. In German.

Jaffe, D.A., Sanders, B.F., 2001. Engineered levee breaches for flood mitigation. Journal of Hydraulic Engineering (ASCE) 127, 471–479.

King, L., Hartmann, H., Gemmer, M., Becker, S., 2004. Der Drei-Schluchten-Staudamm am Yangtze — Ein Großbauprojekt und seine Bedeutung für den Hochwasserschutz. Petermanns Geographische Mitteilungen 148, 26–33.

Kleist, L., Thieken, A.H., Köhler, P., Müller, M., Seifert, I., Borst, D., Werner, U., 2006. Estimation of the regional stock of residential buildings as a basis for comparative risk assessment for Germany. Natural Hazards and Earth System Sciences 6, 541–552.

de Kok, J.L., Grossmann, M., 2010. Large-scale assessment of flood risk and the effects of mitigation measures along the Elbe River. Natural Hazards 52, 143–166. doi:10.1007/s11069-009-9363-6.

Kreibich, H., Thieken, A.H., 2008. Assessment of damage caused by high groundwater inundation. Water Resources Research 44, W09409. doi:10.1029/2007WR006621.

Kuhlmann, B., 2010. Schäden in der Landwirtschaft, in: Thieken, A.H., Seifert, I., Merz, B. (Eds.), Hochwasserschäden. Erfassung, Abschätzung und Vermeidung, oekom, Munich, Germany. pp. 223–234. In German.

LfUG, 2005. Hochwasser in Sachsen. Gefahrenhinweiskarten. Technical Report. Sächsisches Landesamt für Umwelt und Geologie. In German.

Lin, C.A., Wen, L., Lu, G., Wu, Z., Zhang, J., Yang, Y., Zhu, Y., Tong, L., 2010. Real-time forecast of the 2005 and 2007 summer severe floods in the Huaihe River Basin of China. Journal of Hydrology 381, 33–41. doi:10.1016/j.jhydrol.2009.11.017.

LTV, 2010. HWSK-Arbeitsdaten. unpublished. Landestalsperrenverwaltung Sachsen.

LUA, 2002. Das Elbehochwasser im Sommer 2002. Technical Report Heft 73. Landesumweltamt Brandenburg. In German.

Mennis, J., 2003. Generating surface models of population using dasymetric mapping. Professional Geographer 55, 31–42. Type = Article

Merz, B., Elmer, F., Thieken, A., 2009. Significance of "high probability/low damage" versus "low probability/high damage" flood events. Natural Hazards and Earth System Sciences 9, 1033–1046. doi:10.5194/nhess-9-1033-2009.

Merz, B., Kreibich, H., Thieken, A.H., Schmidtke, R., 2004. Estimation uncertainty of direct monetary flood damage to buildings. Natural Hazards and Earth System Sciences 4, 153–163. doi:10.5194/nhess-4-153-2004.

Merz, B., Thieken, A.H., 2009. Flood risk curves and uncertainty bounds. Natural Hazards 51, 437–458. doi:10.1007/s11069-009-9452-6.

MURL, 2000. Hochwasserschadenspotenziale am Rhein in Nordrhein-Westfalen (Flood damage potentials at the river Rhine in North Rhine-Westphalia). Final Report. Ministry of the Environment and Conservation, Agriculture and Consumer Protection of the German State of North Rhine-Westphalia. Düsseldorf, Germany. In German.

Nestmann, F., Büchele, B., 2002. Morphodynamik der Elbe. Final report. Institut für Wassewirtschaft und Kulturtechnik, Universität Karlsruhe. ISBN 3-00-008977-2.

Paik, K., 2008. Analytical derivation of reservoir routing and hydrological risk evaluation of detention basins. Journal of Hydrology 352, 191–201. doi:10.1016/j.jhydrol.2008.01.015. Type = Article

Sanders, B.F., Pau, J.C., Jaffe, D.A., 2006. Passive and active control of diversions to an off-line reservoir for flood stage reduction. Advances in Water Resources 29, 861 – 871. doi:10.1016/j.advwatres.2005.07.015.

Shu, L., Finlayson, B., 1993. Flood management on the lower Yellow River: hydrological and geomorphological perspectives. Sedimentary Geology 85, 285–296.

Thieken, A.H., Kreibich, H., Merz, B., 2006. Improved modelling of flood losses in private households, in: Kundzewicz, Z., Hattermann, F. (Eds.), Natural Systems and Global Change, Polish Academy of Sciences and Potsdam Institute of Climate Impact Research, Poznan, Poland and Potsdam, Germany. pp. 142–150.

Thieken, A.H., Müller, M., Kreibich, H., Merz, B., 2005. Flood damage and influencing factors: New insights from August 2002 flood in Germany. Water Resources Research 41. doi:10.1029/2005WR004177.

Thieken, A.H., Olschewski, A., Kreibich, H., Kobsch, S., Merz, B., 2008. Development and evaluation of FLEMOps - a new *F*lood *L*oss *E*stimation

*MO*del for the *p*rivate *s*ector, in: Proverbs, D., Brebbia, C.A., Penning-Rowsell, E. (Eds.), Flood Recovery Innovation and Response, WIT Press, Southhampton, UK. pp. 315–324.

Thieken, A.H., Seifert, I., Elmer, F., Maiwald, F., Haubrock, S., Schwarz, J., Müller, M., Seifert, J.–O., 2009. Standartisierte Erfassung und Bewertung von Hochwasserschäden. Hydrologie und Wasserbewirtschaftung 53, 198–207.

USACE, 1995. CE-QUAL-RIV1: A Dynamic, One-Dimensional (Longitudinal) Water Quality Model for Streams. Technical Report. Environmental Laboratory, U.S. Army Corps of Engineers. Vicksburg, MS. User's Manual. Final Report.

Vorogushyn, S., Merz, B., Apel, H., 2009. Development of dike fragility curves for piping and micro-instability breach mechanisms. Natural Hazards and Earth System Sciences 9, 1383–1401.

Vorogushyn, S., Merz, B., Lindenschmidt, K.–E., Apel, H., 2010. A new methodology for flood hazard assessment considering dike breaches. Water Resources Research 46, W08541. doi:10.1029/2009WR008475.

WASY, 2005. Untersuchungen zur Optimierung der Flutung der Havelpolder bei Extremhochwässern. Gutachten im Auftrag des Landesumweltamtes Brandenburg. WASY Gesellschaft für Wasserwirtschaftliche Planung und Systemforschung mbH. Unpublished.